Article

Journal of Intelligent Material Systems and Structures

Journal of Intelligent Material Systems and Structures
0(0) 1–7

DOI: 10.1177/1045389X12461720
jim.sagepub.com
SAGE

Geometrical optimization of a hingeless deployment system for an active rotor blade

Alexandre Paternoster[1], Richard Loendersloot[1], Andre de Boer[1] and Remko Akkerman[2]

Abstract

Deployment systems for the Gurney flap need to sustain large centrifugal loads and vibrations while maintaining precisely the displacement under aerodynamic loading. Designing such a mechanism relies on both the actuation technology and the link that transmits motion to the control surface. Flexible beams and piezoelectric patch actuators have been chosen as components to design this mechanism. Flexible beams provide a hingeless robust structure onto which the piezoelectric actuators are bonded. A candidate topology is determined by investigating the compliance of a simple wire structure with beam elements. A parameterized finite element model is then built and optimized for displacement and force through surrogate optimization.

Keywords

actuator, optimization, active composites, morphing, piezoelectric

Introduction

Adapting a rotor blade in flight is the next step toward smarter, more efficient rotorcrafts. The Green Rotorcraft Consortium, part of European Clean Sky Joint Technology Initiative, has chosen the Gurney flap as an active concept to modify the aerodynamic characteristic of a rotor blade during flight (Green Rotorcraft Project Webpage, 2011; Maybury et al., 2010). The Gurney flap consists in a small flap deployed as close as possible to the trailing edge of the blade profile as shown in Figure 1. This flap typically measures 2% of the profile's chord length. It improves the lift of the profile without significant increase in the profile's drag (Maughmer and Bramesfeld, 2008; Thiel and Lesieutre, 2009; Wang et al., 2008). This article presents the optimization work performed on a flexible mechanism to provide sufficient displacement while satisfying the mechanical and deployment time constraints. A procedure is set up to investigate suitable geometries and optimize the geometry of the actuated system.

The active Gurney flap concept

A fully deployed Gurney flap increases the lift coefficient of the profile over a wide range of angles of attack. It also improves both the static and dynamic stall behaviours of the profile (Yee et al., 2007). Helicopter's performances are limited by the lift mismatch between the blade on the advancing side and the blade on the retreating side of the rotorcraft during forward flight.

This problem worsens quickly as the helicopter speed increases because of the quadratic relation between the lift and airspeed. It is solved by reducing the blade angle of attack for the advancing side and increasing it for the retreating side by means of a cyclic pitch control. This is done until the stall limit of the profile is reached. Thus, actively increasing the lift for the retreating blade beyond the capabilities of the profile offers potential for improving the speed and fuel efficiency.

The study carried out by the Green Rotorcraft Consortium's partners concluded that the Gurney flap should be deployed within 10° of blade rotation for optimum performances (Maybury et al., 2010). The blade specifications shown in Table 1 were defined in the project baseline. They provide the data needed to

[1]Applied Mechanics, University of Twente, Enschede, Netherlands
[2]Production Technology, University of Twente, Enschede, Netherlands

Corresponding author:
Alexandre Paternoster, Applied Mechanics, University of Twente, P.O. Box 217, Enschede, 7500 AE, Netherlands.
Email: a.r.a.paternoster@utwente.nl

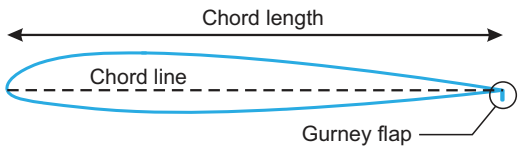

Figure 1. Sketch of the naca 23012 profile with a Gurney flap of 2% long at the trailing edge.

Table 1. Helicopter blade specifications.

Profile reference	Naca23012
Blade radius	8.15 m
Chord length	0.65 m
Rotation speed	26.26 rad/s
Tip speed	214 m/s

Table 2. Design constraints.

Deployment duration	6.6 ms
Axial acceleration	573g
Holding force against the airflow	250 N

derive mechanical constraints for a deployment mechanism (Maybury et al., 2009).

The maximum duration allowed for the deployment mechanism is derived from the blade rotation speed. The mechanism is designed in the plane perpendicular to the axis of the blade. This ensures that the mechanism motion will not be affected by the centrifugal loads. The maximum force required has been determined using flow simulations for a fully deployed flap (Paternoster et al., 2010). This gives an upper bound for the mechanism holding force in the direction of the airflow. These constraints are summarized in Table 2.

Actuators suitable in rotorcrafts

The pneumatic and hydraulic actuators are widely used in aircraft but are unsuitable for rotorcraft actuation due to the space available and their weight. The coil actuators and screw jack electrical motors are more flexible, but the large centrifugal loads caused by the blades rotation limit the use of moving and rotating parts inside a rotor blade. Therefore, an extensive review at the capabilities of piezoelectric-based actuators was carried out in the scope of this project (Maybury et al., 2010; Paternoster et al., 2010).

Piezoelectric actuator expands or contracts when subjected to an electrical field (Chopra, 2002). The strain deforming the piezoelectric material is related to the strain-charge piezoelectric coefficients of the matrix $[d]$ in the mechanical and electrical constitutive equations

$$\{S\} = [s^E]\times\{T\} + [d]^T\times\{E\} \quad (1)$$

$$\{D\} = [d]\times\{T\} + [\in^T]\times\{E\} \quad (2)$$

where S is the strain vector, $[s^E]$ is the compliance matrix under constant electrical field, $\{T\}$ is the stress vector, $[d]$ is the piezoelectric matrix, $[\in^T]$ is the permittivity matrix under constant stress, $\{D\}$ is the dielectric displacement vector and $\{E\}$ is the electrical field vector. The first equation relates the mechanical strain in the material to the applied voltage. Therefore, in the absence of mechanical loading on the piezoelectric component, equation (1) becomes

$$\{S\} = [d]^T\times\{E\} \quad (3)$$

Piezoelectric material's properties are anisotropic. The coefficients of the piezoelectric matrix depend therefore on the poling direction. By convention, axis 3 is the poling direction. Developing equation (3) gives

$$\begin{Bmatrix} \varepsilon_1 \\ \varepsilon_2 \\ \varepsilon_3 \\ \gamma_{23} \\ \gamma_{31} \\ \gamma_{12} \end{Bmatrix} = \begin{bmatrix} 0 & 0 & d_{31} \\ 0 & 0 & d_{32} \\ 0 & 0 & d_{33} \\ 0 & d_{25} & 0 \\ d_{15} & 0 & 0 \\ 0 & 0 & 0 \end{bmatrix} \times \begin{Bmatrix} E_1 \\ E_2 \\ E_3 \end{Bmatrix} \quad (4)$$

The static performance of the material is defined by the maximum strain the material can achieve when unloaded and the largest stress when constrained. They both depend on the value of the strain coefficients ($[d]$) filling the piezoelectric matrix. The d_{33} coefficient is generally the highest coefficient (Chopra, 2002). Therefore, the piezoelectric actuators taking advantage of the d_{33} coefficient achieve the best performance. 'Macrofibre composite' (MFC) actuators consist in piezoelectric fibres embedded in an epoxy matrix as shown in Figure 2. Electrical fields are applied along the piezoelectric fibres, in line with the d_{33} coefficient, through interdigitated electrodes. During the actuator selection process, d_{33} piezoelectric actuators showed the best free strain, block force and actuation speed

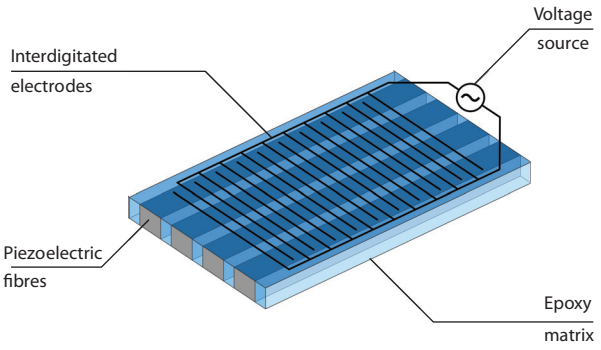

Figure 2. Structure of a 'macrofibre composite' actuator.

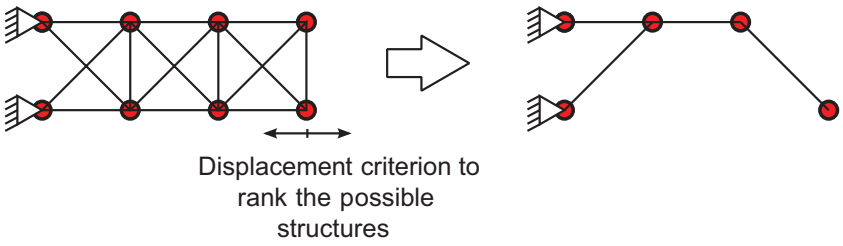

Figure 3. Resulting structure after investigating the flexibility of various configurations.

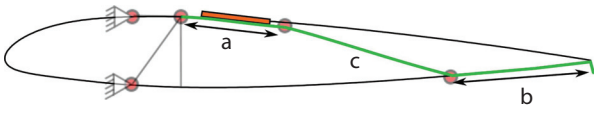

Figure 4. Geometrical parameters used for the finite element analysis. a: length of the upper arm, b: length of the lower arm, and c: curvature of the middle arm.

(Maybury et al., 2010; Paternoster et al., 2010). Their actuation speed met the deployment duration required according to the blade rotation speed. Furthermore, these components have already been used to provide active twist of helicopter blades ensuring their toughness is sufficient to withstand large centrifugal loads (Riemenschneider et al., 2010; Shin et al., 2008). The MFCs are used in this study as the piezoelectric active material. Nevertheless, the displacement generated by piezoelectric actuators is very small. A supporting mechanism has to be conceived to support the MFC actuator and enhance its displacement.

Mechanisms made with bending beams

To provide a sufficiently large displacement, piezoelectric actuators are often bonded onto bending beams. When a voltage is applied, the piezoelectric patch generates strain at the beam surface, which bends the beam. The tip displacement of the bending system is much larger than the displacement generated by the patch actuators. This article details the geometrical optimization of flexible mechanisms consisting of multiple bending beams actuated by piezoelectric patches.

Methods

The early designs of a mechanism made for the Gurney flap consist in directly deploying the Gurney flap transverse to the flow direction (Thiel, 2006; Thiel and Lesieutre, 2009). The efficiency of the Gurney flap as a lift improvement control surface depends strongly on the Gurney flap position relative to the trailing edge. It has been shown that the Gurney flap efficiency is maximized when placed at the trailing edge (Thiel, 2006). However, the space available inside a beam profile is very limited close to the trailing edge. Therefore, a horizontal motion is needed on top of a vertical motion to deploy and place the Gurney flap at the trailing edge. It is possible to kinematically link the vertical motion to the horizontal displacement by a sliding mechanism. Therefore, a single horizontal motion could deploy and bring the Gurney flap at the right position. Moreover, a sliding mechanism allows a cross-flow deployment, which requires less force than deploying the Gurney flap by rotation like a typical control surface. This part describes the process followed to determine a topology and optimize a piezoelectric actuated system.

Topology investigation

The possible topologies for the structural mechanism are investigated using a simplified wired structure with a limited number of nodes. A procedure tests the various possible connections between a defined square array of nodes as shown in Figure 3. A few constraints govern the connections between the nodes: the two fixed nodes and the lower right node must remain connected to the structure. Once the connections are set, a linear system of equations is solved to calculate the deformation of the structure when a horizontal force is applied on the lower right node. The structures are ranked by the amount of horizontal displacement they could offer. This preliminary test leads to the structure displayed in Figure 3.

Finite element model

From the resulting topology, a finite element model (FEM) is made using the same set of connections as shown in Figure 4. The piezoelectric physics environment from COMSOL Multiphysics is used for the implementation, which solves the full electromechanical coupling as formulated by the constitutive equations (equations (1) and (2)). The finite element simulation is a quasi-static bidimensional simulation. The geometry of the structure is generated based on three parameters: the length of the upper arm, the length of the bottom arm and the curvature of the middle arm. The piezoelectric component's length is linked to the length of the upper arm to maximize the space taken by the

Table 3. Characteristics of MFC 4010-P1 from smart material.

Active thickness (mm)	10
Maximum voltage (V)	1500
Electrode spacing (μm)	500
Piezoelectric fibre d_{33} coefficient (pC/N)	460
Free strain per volt (μstrain/V)	0.93

MFC: macrofibre composite.

piezoelectric component for each geometrical configuration. The material's properties are set to the MFC characteristics from the manufacturer datasheets as shown in Table 3 (Smart Material Website, 2011).

The left side of the upper arm is clamped. The lower arm is subjected to a sliding boundary condition meaning displacement is constrained in the direction normal to the bottom surface of the arm. The geometry of both the arms follows the curvature of the profile to use as much available space as possible. The geometry being different for each set of parameters, the number of elements can significantly vary. The quadratic triangular elements utilized are generated based on the thickness of the piezoelectric element and the thickness of each bending arm to have a consistent mesh quality between simulations. On average, 5000 elements are generated for each simulation.

The FEM is embedded inside a procedure that returns the objective value that is going to be maximized by the optimization loop. This objective value is calculated according to the required constraints for the mechanism. The objective value is expressed as

$$y = \sqrt{\left(\frac{d}{d_{pzt}}\right)^2 + \left(\frac{f}{f_{pzt}}\right)^2} \tag{5}$$

where y is the objective value, d is the free displacement of the lower arm, d_{pzt} is the free displacement of the MFC actuator without structure, f is the block force of the mechanism and f_{pzt} is the block force of the MFC actuator without structure. Maximizing this objective leads to mechanisms with both large forces and displacements.

Optimization scheme

The optimization scheme chosen is a surrogate optimization for its flexibility and the number of simulation it requires to approach the optimum. It consists in the determination of a surrogate function followed by a refinement of the optimum (Akcay Perdahcioglu, 2010) as shown in Figure 5. Thirty finite element simulations are computed to explore the design space. A Latin hypercube distribution is chosen to get a relevant distribution of the design parameters. An ordinary kriging model is chosen as a surrogate function to estimate the model (Forrester et al., 2008) and can be

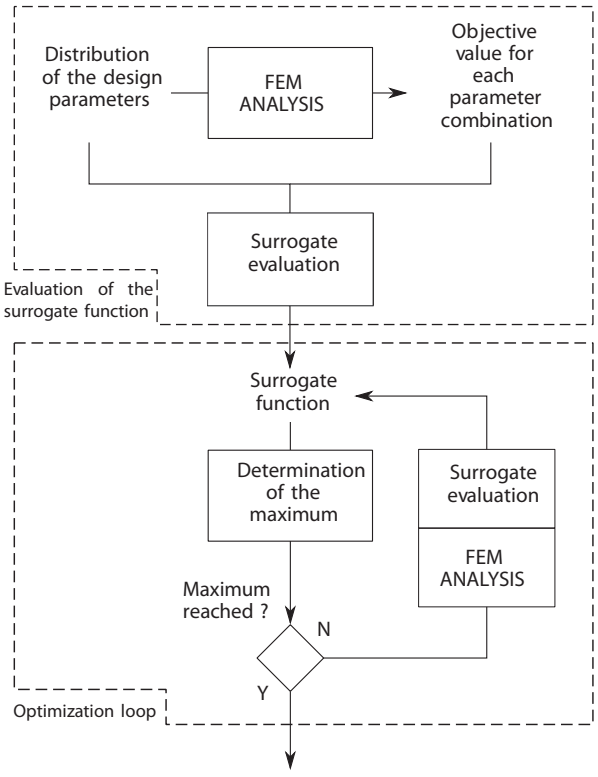

Figure 5. Flow chart detailing the evaluation of the surrogate function and the optimization loop.
FEM: finite element model.

defined as a base function, which represents the global trend of the data with a stochastic function that approximates the data computed at the sampling points

$$\hat{y}(x) = \mu + \in (x) \tag{6}$$

$$x = \begin{pmatrix} a \\ b \\ c \end{pmatrix} \tag{7}$$

where $\hat{y}(x)$ is the estimation of the surrogate function for a vector of parameters x, μ is a constant value corresponding to the base function of the ordinary kriging model and $\in (x)$ is the function that estimates the data modelled at the sampling points. The surrogate function evaluates the objective value for a set of design parameters. After the surrogate function is calculated (cf. Appendix 1), MATLAB standard genetic algorithm searches the design space for a global maximum. The maximum is refined by a gradient-based search. Once the extremum is found, a new finite element analysis evaluates the displacement at the extremum. The loops stop when the objective set no longer improves significantly between two iterations. For this optimization scheme, the termination objective was less than 0.05% of improvement between two iterations. The combination of global and local search strategies ensures the

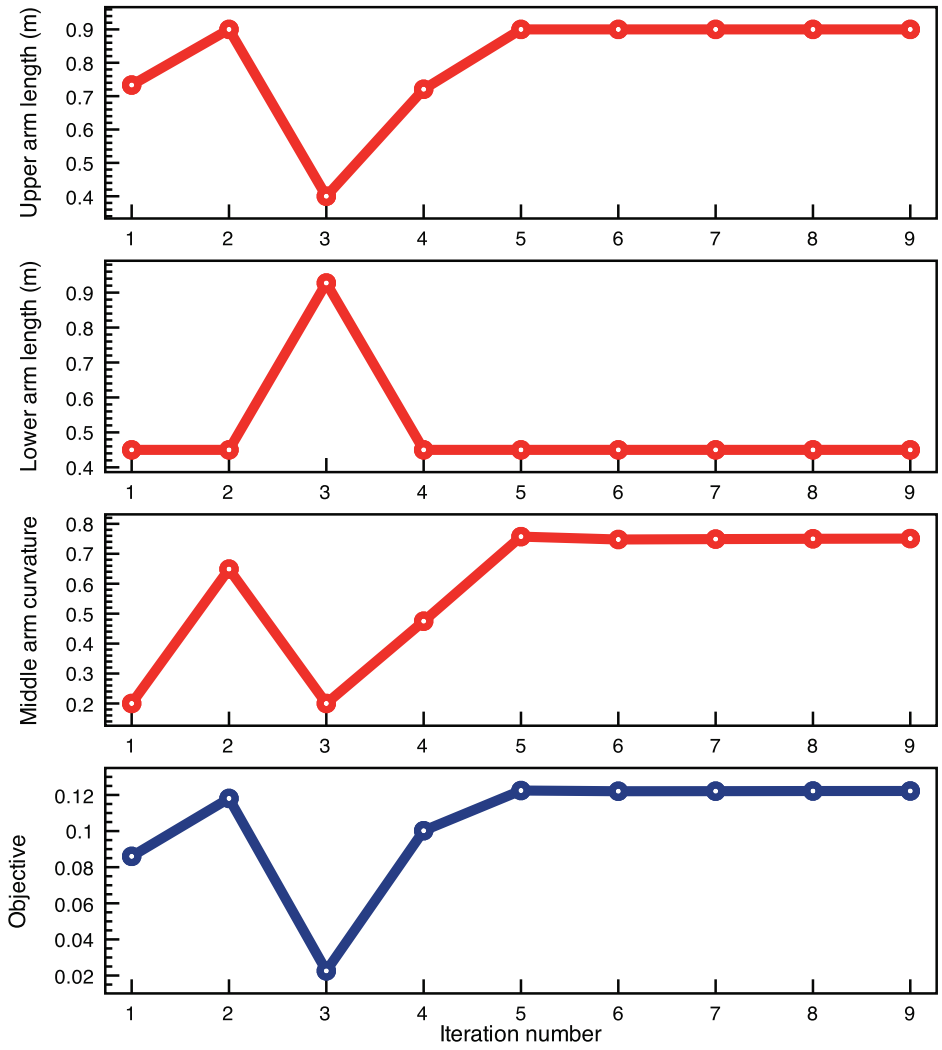

Figure 6. Values of the geometrical parameters used for the optimization and the objective. The curvature is defined by a dimensionless parameter related to the relative position of a node for creating the geometry primitives.

uniqueness of the solution over the design space considered.

Performance evaluation

The force and displacement are not the only requirements. As mentioned in the 'Introduction' section, the deployment duration is critical for a correct performance of the Gurney flap. The force and displacement capabilities of the mechanism are evaluated during the finite element analysis to calculate the objective value. However, a transient analysis is needed to obtain the displacement speed. It is performed on the optimized geometry.

Results

The results of the geometrical optimization are presented in Figure 6. After 30 initial finite element simulations and the evaluation of the surrogate model, the problem converged quickly. The termination criterion is achieved within nine iteration loops. The optimum geometry displayed in Figure 7 shows a middle arm with an opposite slope when compared to the initial structure shown in Figure 3.

The bender mechanism achieves a free displacement of 2.3 mm for a block force of 230 N. The deformed structure is shown in Figure 7. The displacement remains insufficient for sliding directly along the length of the Gurney flap (13 mm). However, the block force is sufficient to sustain the force of the airflow close to the tip of the blade (Paternoster et al., 2010). The objective function can be modified to put more importance on the force or the displacement criterion by adding coefficients in front of the normalized displacement and force. However, modifying the objective function to give more importance to the displacement does not improve the displacement sufficiently to meet the specifications while the force becomes too weak to withstand the airflow force.

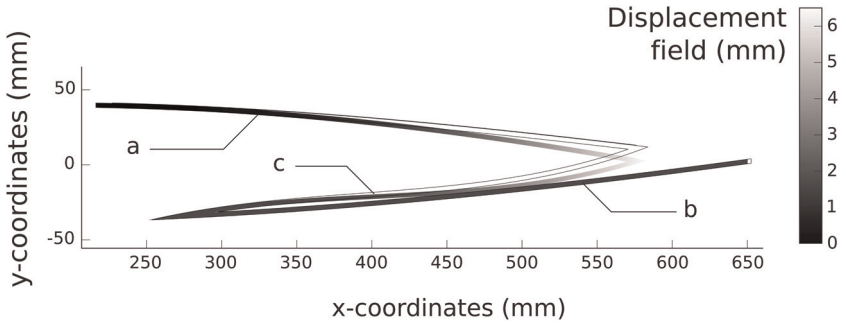

Figure 7. Deformation field of the optimized mechanism with a, b and c being the upper, lower and middle arm, respectively.

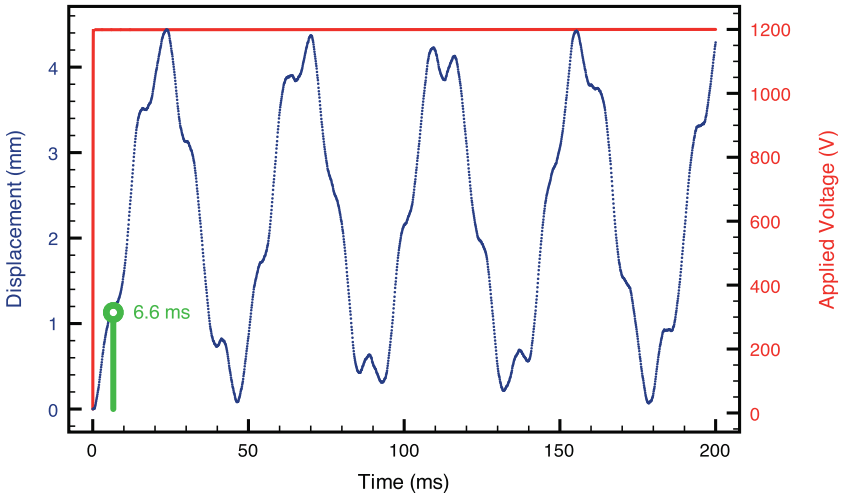

Figure 8. Displacement of the bender mechanism during the transient analysis.

This optimization objective was focused on getting a structure that would maximize both force and displacement. A deployment within 10° of blade rotation is also needed to have a suitable actuation mechanism. This characteristic was investigated for the deployment mechanism using a transient analysis of the finite element analysis set. The displacement of the bender mechanism subjected to a short-step voltage (0.1 ms) is displayed in Figure 8. Ten degrees of sweeping angle are completed in 6.6 ms. The displacement shown at this time step is 1.13 mm. The free displacement is achieved at 11 ms and increases further on due to the inertia of the motion. The displacement oscillations are undamped because no structural damping has been implemented in the FEM.

Conclusion and future work

The process described in this article successfully achieves to optimize an actuation mechanism according to both displacement and force. It manages to amplify the small strain generated in an MFC piezoelectric actuator into a significant displacement. The performance of the resulting geometry showed sufficient block force. However, the displacement and the deployment duration are still not sufficient for this application. The transient analysis shows that the displacement of the structure is higher than the free displacement using the inertia of the motion. Future work involves redefining the objective's calculation to include and take advantage of the dynamic effects and implementing a more complex FEM that takes into account damping, contact elements and has more MFCs. The described procedure can be applied to any actuated system requiring an optimization based on performances.

Funding

This project is funded by the Clean Sky Joint Technology Initiative (grant number [CSJU-GAM-GRC-2008-001]9) - GRC1 Innovative Rotor Blades, which is part of the European Union's 7th Framework Program (FP7/2007-2013).

References

Akcay Perdahcioglu D (2010) *Optimizing the dynamic behavior of structures using substructuring and surrogate modeling*. PhD Thesis, University of Twente, Enschede, Netherlands.

Chopra I (2002) Review of state of art of smart structures and integrated systems. *AIAA Journal* 40(11): 2145–2187.

Forrester A, Sóbester A and Keane A (2008) *Engineering Design via Surrogate Modelling: A Practical Guide*, Chichester, West Sussex, UK: John Wiley & Sons Ltd.

Green Rotorcraft Project Webpage (2011) CleanSky – Green Rotorcraft. Available at: http://www.cleansky.eu/index.php?arbo_id=69 set_language=en

Maughmer MD and Bramesfeld G (2008) Experimental investigation of Gurney flaps. *Journal of Aircraft* 45(6): 2062–2067.

Maybury W, D'Andrea A, Hilditch R, et al. (2009) *Baseline blade definition for GRC1.1*. CS JU/ITD GRC/RP/1.1/31002, Green Rotorcraft, 6 February 2009.

Maybury W, Visingardy A, van't Hoff SC, et al. (2010) *GRC1.1 technology review document*. CS JU/ITD GRC/RP/1.1/31005, Green Rotorcraft, 16 February 2010.

Paternoster A, de Boer A, Loendersloot R, et al. (2010) Actuators for smart applications. *Proceedings of the ASME 2010 Conference on Smart Materials, Adaptive Structures and Intelligent Systems, Philadelphia, Pennsylvania,* 28 September–1 October, 2010: 673–679.

Riemenschneider J, Opitz S, Schulz M, et al. (2010) Active twist rotor for wind tunnel investigations. *Proceedings of the ASME 2010 Conference on Smart Materials, Adaptive Structures and Intelligent Systems, Philadelphia, Pennsylvania,* 28 September–1 October, 2010: 371–378.

Shin SJ, Cesnik CES, Wilkie WK, et al. (2008) Design and manufacturing of a model-scale active twist rotor prototype blade. *Journal of Intelligent Material Systems and Structures* 19(12): 1443–1456.

Smart Material Website (2011) Macro fiber composite – MFC. Available at: http://www.smart-material.com/MFC-product-main.html

Thiel M (2006) Actuation of an active Gurney flap for rotorcraft applications. MSc Thesis, The Pennsylvania State University, State College, PA.

Thiel M and Lesieutre G (2009) New actuation methods for miniature trailing-edge effectors for rotorcraft. In: *AIAA/ASME/ASCE/AHS/ASC structures, structural dynamics, and materials conference*, Palm Springs, California, 4–7 May.

Wang J, Li Y and Choi K (2008) Gurney flap – lift enhancement, mechanisms and applications. *Progress in Aerospace Sciences* 44(1): 22–47.

Yee K, Joo W and Lee DH (2007) Aerodynamic performance analysis of a Gurney flap for rotorcraft application. *Journal of Aircraft* 44(3): 1003–1014.

Appendix 1

Calculation of the surrogate function with an ordinary kriging model

An ordinary kriging model can be defined as a base function, which represents the global trend of the data with a stochastic function that approach the data computed at the sampling points.

A kriging model can be defined as

$$\hat{y}(x) = \mu + \in (x) \tag{8}$$

where $\hat{y}(x)$ is the estimation of the surrogate function for a set of parameters x, μ is a constant value corresponding to the base function of the ordinary kriging model and $\in (x)$ is the function that estimates the data modelled at the sampling points. The surrogate function will evaluate the horizontal displacement of the bottom arm for a set of design parameters.

A Gaussian correlation is used for this model

$$R(x_i, x_j) = e^{-\theta(x_i - x_j)^2} \tag{9}$$

where x_i and x_j are parameter values and θ is a scaling parameter for the correlation function, whose value depends on the problem considered.

Then the base function is estimated as

$$\hat{\mu} = \frac{X^T \hat{R}^{-1} y}{X^T \hat{R}^{-1} X} \tag{10}$$

where $\hat{\mu}$ is the estimation of the base function, $\hat{R}$ is the correlation matrix and X is a unit vector (ordinary kriging case).

Therefore, the prediction of the kriging model is

$$\hat{y} = \hat{\mu} + r^T \hat{R}^{-1}(y - \mathbb{I}\,\hat{\mu}) \tag{11}$$

where $\hat{y}$ is the estimation of y, r is the correlation vector between the set of parameters, y is evaluated at and the parameters at which the surrogate function has been evaluated and $\mathbb{I}$ is a unit vector.